

The combinatorial PT-DT correspondence

Helen Jenne^{*1}, Gautam Webb^{†2}, and Benjamin Young^{‡2}

¹CNRS, Institut Denis Poisson, Université de Tours and Université d'Orléans, France

²Department of Mathematics, University of Oregon, Eugene, OR, USA

Abstract. We resolve a conjecture from algebraic geometry, which states that two generating functions for plane partition-like objects (the “box-counting” formulae for the Calabi–Yau topological vertices in Donaldson–Thomas theory and Pandharipande–Thomas theory) are equal up to a factor of MacMahon’s generating function for plane partitions. The main tools in our proof are a Desnanot–Jacobi-type “condensation” identity, and a novel application of the tripartite double-dimer model of Kenyon–Wilson.

Keywords: Double-dimer model, Desnanot–Jacobi identity, Donaldson–Thomas theory, Pandharipande–Thomas theory, plane partitions

1 Introduction

Donaldson–Thomas (DT) theory and Pandharipande–Thomas (PT) theory are branches of enumerative geometry closely related to mirror symmetry and string theory. In both theories, generating functions arise known as the *combinatorial Calabi–Yau topological vertices*. These generating functions enumerate seemingly different plane partition-like objects. In this paper, we prove that the generating functions coincide up to a factor of $M(q)$, MacMahon’s generating function for plane partitions [5]. Our result, taken together with a substantial body of geometric work, proves a geometric conjecture in the foundational work of Pandharipande–Thomas theory which has been open for over 10 years.

The generating function from Donaldson–Thomas theory is known as the DT topological vertex. Denoted $V(\mu_1, \mu_2, \mu_3)$, where each μ_i is a partition, it counts plane partitions *asymptotic to* μ_1, μ_2 , and μ_3 (see Section 3.1). The PT topological vertex, denoted by $W(\mu_1, \mu_2, \mu_3)$, is a generating function for a certain class of finitely generated $\mathbb{C}[x_1, x_2, x_3]$ -modules (see Section 4.1).

We prove that

^{*}helen.jenne@lmpt.univ-tours.fr. Helen Jenne has received funding from the European Research Council (ERC) through the European Union’s Horizon 2020 research and innovation programme under the Grant Agreement No 759702.

[†]gwebb@uoregon.edu

[‡]bjy@uoregon.edu. Benjamin Young was partially supported by the Knut and Alice Wallenberg Foundation Grant KAW:2010.0063.

Theorem 1.1 ([11, Calabi–Yau case of Conjecture 4]).

$$V(\mu_1, \mu_2, \mu_3) = M(q)W(\mu_1, \mu_2, \mu_3), \quad (1.1)$$

where $M(q) = \prod_{i \geq 1} (1 - q^i)^{-i}$.

The geometric corollary of this theorem is a proof of Theorem/Conjecture 2 of [11], which, loosely speaking, states that $W(\mu_1, \mu_2, \mu_3)$ computes the local contribution to the Pandharipande–Thomas generating function. The proof of this corollary combines Theorem 1.1 with the analogous result in DT theory [6, 7, 9] along with [8, Section 4.1.2]; it is a consequence of the fact that both DT and PT theory give the same invariants as a third theory, Gromov–Witten theory.¹

The combinatorics problems which we solve are stated in the geometry literature as “box-counting” problems; that is, the objects of interest are plane partition-like. The following bijections are well-known:

$$\begin{array}{ccc} \text{dimer configurations on} & & \text{finite-length monomial} \\ \text{the honeycomb graph} & \leftrightarrow \text{plane partitions} \leftrightarrow & \text{ideals in } \mathbb{C}[x_1, x_2, x_3] \end{array}$$

The first one is a 3D version of the correspondence between a partition and its Maya diagram; it is stated explicitly in Section 3.2. We use essentially the same correspondence to give a dimer description of the DT topological vertex $V(\mu_1, \mu_2, \mu_3)$. On the PT side, the correspondences are

$$\begin{array}{ccc} \text{tripartite double-dimer configs.} & \xleftrightarrow{(1)} & \text{labelled box} \\ \text{on the honeycomb graph} & & \text{configurations} \xleftrightarrow{(2)} & \mathbb{C}[x_1, x_2, x_3]\text{-modules} \\ & & & (M_1 \oplus M_2 \oplus M_3) / \langle (1, 1, 1) \rangle \end{array}$$

The correspondence (1) is new, as far as we are aware. We describe labelled box configurations, and the generating functions for them which arise in PT theory, carefully in Section 4. Interestingly, though it is a purely combinatorial correspondence, it is not bijective—rather, it is a weight-preserving, 1-to-many correspondence. Here $M_1 \subseteq \mathbb{C}[x_1, x_1^{-1}, x_2, x_3]$ is spanned by all monomials $x_1^i x_2^j x_3^k$ where $i \in \mathbb{Z}$ and (j, k) ranges over some fixed partition μ_1 , with M_2, M_3 defined similarly; the quotient is killing the diagonal of the direct sum.

The correspondence (2) is incidental to this work and is described in [11]; nor will we need to discuss the structure of the modules in the codomain. We expect that our methods will be relevant in other similar situations (one such situation arises in Rank 2 DT theory [1]) and we would be eager to learn of other instances in which our techniques would apply.

¹In [6, 7, 11] and in general elsewhere in the geometry literature, all of the formulas have q replaced by $-q$. The sign is there for geometric reasons which are immaterial for us.

We prove Theorem 1.1 by observing that both $V(\mu_1, \mu_2, \mu_3)/M(q)$ and $W(\mu_1, \mu_2, \mu_3)$ are the unique solution of the same recurrence, with the same initial conditions. The recurrence in question is called the *condensation recurrence*; we postpone its definition to Section 2, after we have made the required definitions.

Viewed as a recurrence in μ_1 and μ_2 , Equation (2.1) uniquely characterizes V and W . The base case is when one of the three partitions μ_i is equal to zero; Equation (1.1) is known to hold in this situation [11].

When recast in terms of the dimer model, $V(\mu_1, \mu_2, \mu_3)$ is easily seen to satisfy Equation (2.1) by Kuo's *graphical condensation* [4]; this is essentially the content of Section 3.

Showing that $W(\mu_1, \mu_2, \mu_3)$ satisfies Equation (2.1) is considerably more intricate, but once we translate to the double-dimer model, the bulk of the work was done elsewhere, in work of Jenne [2]. Essentially, [2] evaluates a certain determinant by the classical Desnanot–Jacobi identity, and then interprets all six terms in the identity in terms of W .

The full version of this abstract will appear in [3]; proofs have been omitted due to space constraints.

2 Definitions

Fix partitions μ_1, μ_2, μ_3 . For this paper, we identify μ_i with the coordinates of the boxes of its Young diagram, with the corner of the diagram located at $(0, 0)$. Define the following subsets of \mathbb{Z}^3 , thought of as sets of boxes: $\text{Cyl}_1 = \{(x, u, v) \in \mathbb{Z}^3 \mid (u, v) \in \mu_1\}$, $\text{Cyl}_2 = \{(v, y, u) \in \mathbb{Z}^3 \mid (u, v) \in \mu_2\}$, and $\text{Cyl}_3 = \{(u, v, z) \in \mathbb{Z}^3 \mid (u, v) \in \mu_3\}$.

Moreover, let $\mathbb{Z}_{\geq 0}^3$ denote the integer points in the first octant (including the coordinate planes and axes). Let $\text{Cyl}_i^+ = \text{Cyl}_i \cap \mathbb{Z}_{\geq 0}^3$ and $\text{Cyl}_i^- = \text{Cyl}_i \setminus \mathbb{Z}_{\geq 0}^3$. Finally, let

$$\begin{aligned} \text{II}_1 &= \text{Cyl}_2 \cap \text{Cyl}_3 \setminus \text{Cyl}_1, \\ \text{I}^- &= \text{Cyl}_1^- \cup \text{Cyl}_2^- \cup \text{Cyl}_3^-, & \text{II}_2 &= \text{Cyl}_3 \cap \text{Cyl}_1 \setminus \text{Cyl}_2, & \text{II} &= \text{II}_1 \cup \text{II}_2 \cup \text{II}_3, \\ \text{I}^+ &= \text{Cyl}_1^+ \cup \text{Cyl}_2^+ \cup \text{Cyl}_3^+, & \text{II}_3 &= \text{Cyl}_1 \cap \text{Cyl}_2 \setminus \text{Cyl}_3, & \text{III} &= \text{Cyl}_1 \cap \text{Cyl}_2 \cap \text{Cyl}_3. \end{aligned}$$

We will need the following standard notions of Maya diagrams. If $\lambda = (\lambda_1, \lambda_2, \dots, \lambda_k)$ is a partition with k parts, define $\lambda_t = 0$ for $t > k$. The *Maya diagram* of λ is the set $\{\lambda_t - t + \frac{1}{2}\} \subseteq \mathbb{Z} + \frac{1}{2}$. We frequently associate a partition with its Maya diagram by drawing a Maya diagram as a doubly infinite sequence of beads and holes, indexed by $\mathbb{Z} + \frac{1}{2}$, with the beads representing elements of the above set. For instance, the Maya diagrams of the empty partition and of the partition $\lambda = (4, 2, 1)$ are the sets $\{-\frac{1}{2}, -\frac{3}{2}, \dots\}$ and $\{\frac{7}{2}, \frac{1}{2}, -\frac{3}{2}, -\frac{7}{2}, -\frac{9}{2}, \dots\}$, respectively, which are drawn as

$$\dots \circ \circ \circ \circ \mid \bullet \bullet \bullet \dots \quad \text{and} \quad \dots \circ \circ \circ \circ \bullet \circ \circ \bullet \mid \circ \bullet \circ \bullet \bullet \bullet \dots$$

When convenient, we simply mark the location of 0 with a vertical line, rather than labelling the beads with elements of $\mathbb{Z} + \frac{1}{2}$. Conversely, if S is a subset of $\mathbb{Z} + \frac{1}{2}$, define

$S^+ = \{x \in S \mid x > 0\}$ and $S^- = \{x \in \mathbb{Z} + \frac{1}{2} \setminus S \mid x < 0\}$. If both S^+ and S^- are finite, then define the *charge* of S , $c(S)$, to be $|S^+| - |S^-|$; then it is easy to check that the set $\{s - c(S) : s \in S\}$ is the Maya diagram of some partition λ ; we say that S itself is the *charge $c(S)$ Maya diagram* of λ .

If λ is a partition with Maya diagram S , let λ^r (resp. λ^c) be the partition associated to the charge -1 (resp. 1) Maya diagram $S \setminus \{\min S^+\}$ (resp. $S \cup \{\max S^-\}$). Let λ^{rc} be the partition associated to the Maya diagram $(S \setminus \{\min S^+\}) \cup \{\max S^-\}$.

In both PT and DT, it will be convenient to divide the $N \times N \times N$ honeycomb graph $H(N)$ into three sectors and label some of the vertices on the outer face as shown in Figure 1 for $H(3)$. We remark that the division into sectors makes sense as $N \rightarrow \infty$. The reason for these particular choices of labels is that we will need to specify these specific vertices, both in DT and PT, based on the Maya diagrams of various

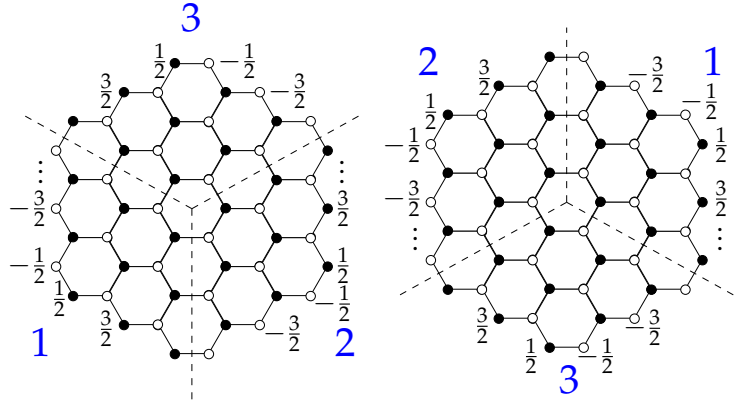


Figure 1: The division of $H(3)$ into sectors for DT and PT partitions.

partitions. Finally, let $X = X(\mu_1, \mu_2, \mu_3)$ be a power series in q , depending on three partitions μ_1, μ_2, μ_3 , which is symmetric with respect to cyclic permutation of these partitions. We will show that V and W are solutions X to the following functional equation:

$$q^C X(\mu_1, \mu_2, \mu_3) X(\mu_1^{rc}, \mu_2^{rc}, \mu_3) = q^C X(\mu_1^{rc}, \mu_2, \mu_3) X(\mu_1, \mu_2^{rc}, \mu_3) + X(\mu_1^r, \mu_2^c, \mu_3) X(\mu_1^c, \mu_2^r, \mu_3). \quad (2.1)$$

Here, $C = 1 + (\mu_1)_{d(\mu_1)} - d(\mu_1) + (\mu_2)_{d(\mu_2)} - d(\mu_2)$, where $d(\lambda)$ is the diagonal of λ . This constant is discussed further in Section 3.3.

Since the partitions $\mu_i^r, \mu_i^c, \mu_i^{rc}$ are all smaller, in some sense, than μ_i , and since none of the topological vertex terms are equal to zero, we can divide both sides of the condensation recurrence by $V(\mu_1^{rc}, \mu_2^{rc}, \mu_3)$ and obtain a recursive characterization of $V(\mu_1, \mu_2, \mu_3)$. Note also that $V(\mu_1, \mu_2, \mu_3) = V(\mu_2, \mu_3, \mu_1)$ by symmetry - so we can say that $V(\mu_1, \mu_2, \mu_3)$ is the *unique* power series which satisfies the condensation recurrence, where we take the base cases to be the (known) values of $V(\mu_1, \mu_2, \emptyset)$ for all partitions μ_1, μ_2 .

3 DT

3.1 DT box configurations

We say that a *plane partition asymptotic to* (μ_1, μ_2, μ_3) is an order ideal under the product order in $\mathbb{Z}_{\geq 0}^3$ which contains $\mathbf{I}^+ \cup \mathbf{II} \cup \mathbf{III}$, together with only finitely many other points in $\mathbb{Z}_{\geq 0}^3$. We let $P(\mu_1, \mu_2, \mu_3)$ denote the set of plane partitions asymptotic to μ_1, μ_2, μ_3 .

If any of μ_1, μ_2, μ_3 are nonzero, then every $\pi \in P(\mu_1, \mu_2, \mu_3)$ is an infinite subset of $\mathbb{Z}_{\geq 0}^3$. We define $w(\pi) = |\pi \setminus (\mathbf{I}^+ \cup \mathbf{II} \cup \mathbf{III})| - |\mathbf{II}| - 2|\mathbf{III}|$, the customary measure of “size” of such a plane partition in the geometry literature (see, for instance, [6]).

Define

$$V(\mu_1, \mu_2, \mu_3) = \sum_{\pi \in P(\mu_1, \mu_2, \mu_3)} q^{w(\pi)}.$$

We call $V(\mu_1, \mu_2, \mu_3)$ the *topological vertex in Donaldson–Thomas theory*. Note that if $\pi \in P(\emptyset, \emptyset, \emptyset)$ with $|\pi| = n$, then π is a plane partition of n in the conventional sense, that is, a finite array of integers such that each row and column is a weakly decreasing sequence of nonnegative integers. Thus MacMahon’s enumeration of plane partitions [5] gives us $V(\emptyset, \emptyset, \emptyset) = \prod_{i=1}^{\infty} (1 - q^i)^{-i}$.

In [10], there is an expansion of $V(\mu_1, \mu_2, \mu_3)$ in terms of Schur functions. However, since no similar expansion is known in PT theory, this expansion does not help prove Theorem 1.1.

3.2 DT theory and the dimer model

Before giving the dimer description of $V(\mu_1, \mu_2, \mu_3)$, we review the correspondence between plane partitions and dimer configurations of a honeycomb graph. By representing each integer i in a plane partition as a stack of i unit boxes, a plane partition can be visualized as a collection of boxes which is stacked stably in the positive octant, with gravity pulling them in the direction $(-1, -1, -1)$. This collection of boxes can be viewed as a lozenge tiling of a hexagonal region of triangles, which is equivalent to a dimer configuration (also called a perfect matching) of its dual graph.

Just as a plane partition can be visualized as a collection of boxes, a plane partition asymptotic to (μ_1, μ_2, μ_3) can be visualized as a collection of boxes, as shown in Figure 2, left picture. Moreover, a version of the above correspondence puts these box collections in bijection with dimer configurations on the honeycomb graph $H(N)$ with some outer vertices removed, which we call $H(N; \mu_1, \mu_2, \mu_3)$. Specifically, $H(N; \mu_1, \mu_2, \mu_3)$ is constructed as follows. Let S_i be the Maya diagram of μ_i . Construct the sets S_i^+, S_i^- for $i = 1, 2, 3$ and then remove the vertices with the labels in $S_i^+ \cup S_i^-$ from sector i of $H(N)$ (here, we are referring to the labelling of the boundary vertices illustrated in Figure 1, left picture).

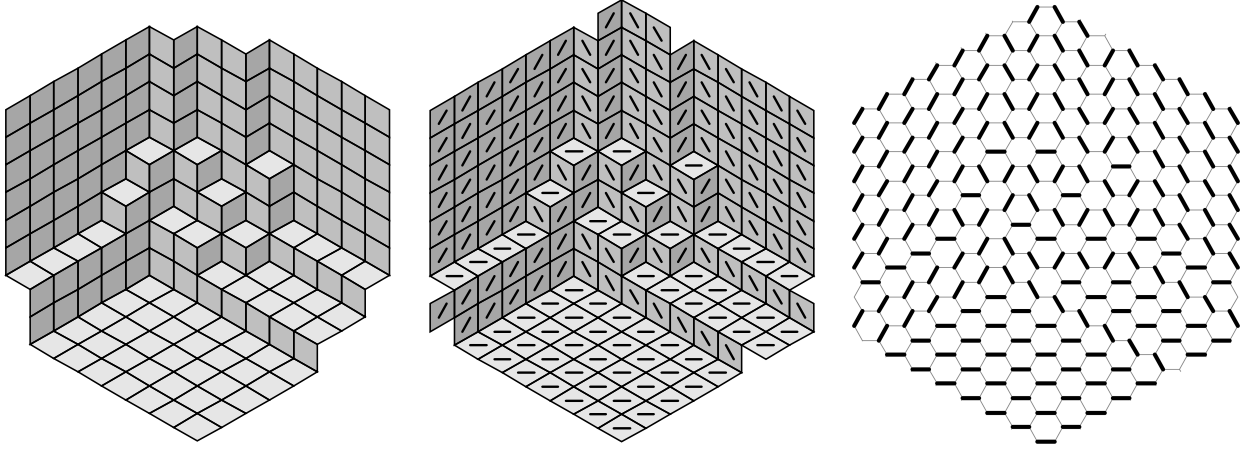


Figure 2: Shown left is a plane partition π asymptotic to (μ_1, μ_2, μ_3) , where $\mu_1 = (1, 1)$, $\mu_2 = \mu_3 = (2, 1, 1)$, $|\text{II}| = 6$, $|\text{III}| = 3$, and $w(\pi) = 13 - |\text{II}| - 2|\text{III}| = 1$. We see that π is equivalent to a tiling, which is truncated in the center image so that it corresponds to a dimer configuration of $H(7)$ with a few vertices on the outer face deleted.

3.3 The condensation recurrence in DT theory

We now show that the DT partition function satisfies the condensation recurrence; this is now a corollary of the well-known “graphical condensation” theorem of Kuo:

Theorem 3.1 ([4, Theorem 5.1]). *Let $G = (V_1, V_2, E)$ be a planar bipartite graph with a given planar embedding in which $|V_1| = |V_2|$. Let vertices a, b, c , and d appear in a cyclic order on a face of G . If $a, c \in V_1$ and $b, d \in V_2$, then*

$$Z^D(G)Z^D(G - \{a, b, c, d\}) = Z^D(G - \{a, b\})Z^D(G - \{c, d\}) + Z^D(G - \{a, d\})Z^D(G - \{b, c\}).$$

Take G to be $H(N; \mu_1^r, \mu_2^c, \mu_3)$ for N sufficiently large². Let a and b be the vertices in sector 1 labelled by $\max S_1^-$ and $\min S_1^+$, respectively. Similarly, we let c and d be the vertices in sector 2 labelled by $\max S_2^-$ and $\min S_2^+$. Then $G - \{a, b, c, d\}$ is $H(N; \mu_1, \mu_2, \mu_3)$.

The resulting six dimer-model partition functions are all instances of the topological vertex, up to order N . The normalization constant q^C arises because the “folklore” technique which associates a plane partition to a dimer configuration preserves the weight up to a factor of $q^{w(\pi_{\min})}$, where π_{\min} is the minimal dimer configuration. The weight of this configuration is computed, for instance in [4]; for us the computation is substantially messier, as $w(\pi_{\min})$ depends on μ_1, μ_2, μ_3 in a delicate way; we omit the details.

²A sufficient lower bound for N depends on μ_1, μ_2 , and μ_3 .

4 PT

4.1 Labelled AB configurations

In this section we introduce one of the main objects of our study: labelled AB configurations.

Definition 4.1. If $A \subseteq \Gamma^- \cup \text{III}$ and $B \subseteq \text{II} \cup \text{III}$ are finite sets of boxes, then (A, B) is an AB configuration if the following condition is satisfied:

If $w = (w_1, w_2, w_3)$ is a cell in $\Gamma^- \cup \text{III}$ (resp. $w \in \text{II} \cup \text{III}$) and any cell in $\{(w_1 - 1, w_2, w_3), (w_1, w_2 - 1, w_3), (w_1, w_2, w_3 - 1)\}$ supports a box in A (resp. B), then w must support a box in A (resp. B).

We remark that this is the familiar condition for plane partitions, except that gravity is pulling the boxes in the direction $(1, 1, 1)$, away from the origin.

Next, we give an algorithm that labels AB configurations. Note that the algorithm assigns labels to cells, not boxes.

Algorithm 4.2.

1. If a connected component of $(\Gamma^- \cap A) \cup (\text{II} \setminus B) \cup (\text{III} \cap (A \Delta B))$ contains a box in $\text{Cyl}_i^- \cup \text{II}_i^-$ and a box in $\text{Cyl}_j^- \cup \text{II}_j^-$, where $i \neq j$, terminate with failure.
2. For each connected component C of $(\Gamma^- \cap A) \cup (\text{II} \setminus B) \cup (\text{III} \cap (A \Delta B))$ that contains a box in $\text{Cyl}_i^- \cup \text{II}_i^-$, label each element of C by i .
3. For each remaining connected component C of $(\Gamma^- \cap A) \cup (\text{II} \setminus B) \cup (\text{III} \cap (A \Delta B))$, label each element of C by the same freely chosen element of \mathbb{P}^1 .

Because the algorithm may fail in Step 1, there are AB configurations that cannot be labelled. A *labelled AB configuration* is an AB configuration for which the labelling algorithm succeeds. Let $\mathcal{AB}(\mu_1, \mu_2, \mu_3)$ denote the set of all labelled AB configurations.

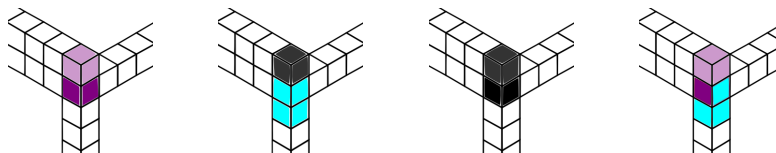


Figure 3: The AB configurations from Example 4.3

Example 4.3. Let $\mu_1 = (1)$, $\mu_2 = (2)$, and $\mu_3 = (1)$. Then $\text{III} = \{(0, 0, 0)\}$ and $\text{II} = \text{II}_1 = \{(0, 0, 1)\}$. In Figure 3 we illustrate four AB configurations³, three of which are labelled AB configurations.

³The first three of these configurations appear in [11, Section 5.4] as the length 1 configuration (i), the length 3 configuration (iv), and the length 2 configuration (iii).

1. A consists of a single box at $(0,0,0)$ and $B = \emptyset$. Step 2 of Algorithm 4.2 gives the cells $(0,0,0)$ and $(0,0,1)$ the label 1, which is indicated by the color purple. The cell $(0,0,0)$ is opaque because it supports a box; the cell $(0,0,1)$ does not.
2. $A = \{(0,0,0), (0,0,-1)\}$ and $B = \{(0,0,1)\}$. Step 2 labels the cells in A by 3, which we illustrate by coloring the two boxes cyan. The box at $(0,0,1)$ is colored gray because it does not get a label.
3. $A = \emptyset$ and $B = \{(0,0,0), (0,0,1)\}$. Again, the box at $(0,0,1)$ does not get a label. The box at $(0,0,0)$ has a free choice of label in \mathbb{P}^1 .
4. $B = \emptyset$ and $A = \{(0,0,0), (0,0,-1)\}$. The algorithm terminates with failure in Step 1 because $(0,0,-1) \in \text{Cyl}_3^-$ and $(0,0,1) \in \text{II}_1^-$. In the figure, $(0,0,0)$ is colored both cyan, required by the box at $(0,0,-1)$, and purple, required by the cell at $(0,0,1)$.

Example 4.4. Shown in Figure 4 is a labelled AB configuration with $\mu_1 = (3,3,1)$, $\mu_2 = (3,2,2,1)$, and $\mu_3 = (5,3,3,1)$. The left image shows the configuration. The boxes belonging to A are marked; all other boxes are in B . The right image includes surrounding cells in II . In both images, yellow cells are labelled 2 and purple cells are labelled 1. Opaque cells support a box in the configuration and transparent cells do not. The two connected components labelled by a freely chosen element of \mathbb{P}^1 are colored black and orange, respectively.

Define

$$W(\mu_1, \mu_2, \mu_3) = \sum_{(A,B) \in \mathcal{AB}(\mu_1, \mu_2, \mu_3)} q^{|A|+|B|}.$$

We prove, in a paper in preparation, that labelled AB configurations are a discrete version⁴ of *labelled box configurations* as defined in [11, Section 2.5], and therefore $W(\mu_1, \mu_2, \mu_3)$ is the *topological vertex in PT theory*.

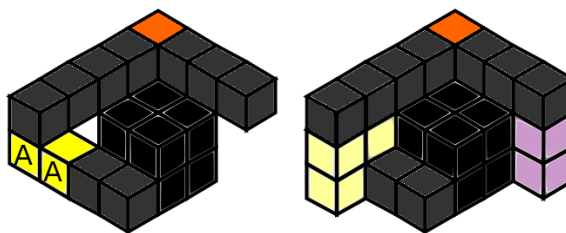


Figure 4: The AB configuration from Example 4.4

4.2 PT theory and the labelled double-dimer model

Next we explain the relationship between labelled AB configurations and *double-dimer configurations*. On an infinite graph, a double-dimer configuration is the union of two dimer configurations.

Let (A, B) be an AB configuration. We consider A and B separately. For A , we view the surface $(\text{I}^- \cup \text{III}) \setminus A$ as a lozenge tiling. In other words, we take the set of boxes

⁴More precisely, there is a surjection ψ from labelled AB configurations to labelled box configurations, and if π is a labelled box configuration, $|\psi^{-1}(\pi)| = \chi_{\text{top}}(\pi)$, where $\chi_{\text{top}}(\pi)$ is the topological Euler characteristic of the moduli space of labellings of π , in the terminology of [11].

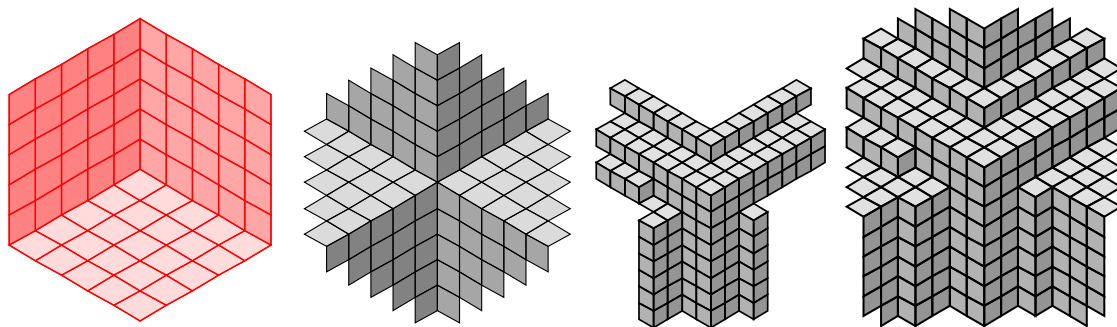


Figure 5: Converting an AB configuration to a tiling of the plane. Left two pictures: extra tiles that may be used to extend tilings for B and A , respectively. Right two pictures: an example of the surface $(I^- \cup III) \setminus A$, and its extended tiling.

$A \subseteq I^- \cup III$ and draw the tiles corresponding to cells that are not in A . Similarly, for B , we view the surface $(II \cup III) \setminus B$ as a lozenge tiling. We then extend each of these tilings to tilings of the entire plane. That is, in Figure 5, we overlay the third image on the second image to obtain the final image. Then, these lozenge tilings are equivalent to dimer configurations of the infinite honeycomb graph H .

Let M_A (resp. M_B) denote the dimer configuration of H corresponding to the infinite tiling obtained from A (resp. B). Superimposing M_A and M_B so that Region III is in the same place in the two pictures produces a double-dimer configuration $D_{(A,B)}$ on H .

For example, the third image of Figure 5 shows the tiling corresponding to A , where (A, B) is the AB configuration from Figure 4. The set A consists of two boxes, $(3, -1, 0)$ and $(3, 0, 0)$, so we have drawn the tiles corresponding to $(I^- \cup III) \setminus \{(3, -1, 0), (3, 0, 0)\}$.

The corresponding dimer configurations M_A and M_B are shown in Figure 6. Their superposition, shown immediately to their right, is a double-dimer configuration on H .

Just as we label certain AB configurations, we label certain double-dimer configurations. Before presenting our double-dimer labelling algorithm, we make a few remarks. It can be shown that each path in $D_{(A,B)}$ crosses each coordinate axis finitely many times. Consequently, there is a well-defined notion of the sectors⁵ that contain the ends of such a path. Also, let $h_{(A,B)}$ be the relative height function that assigns to each face f of H the height difference at f of the surface corresponding to M_B above that corresponding to M_A . The loops and paths in $D_{(A,B)}$ are the contour lines for $h_{(A,B)}$.

Let F be the set of faces of H . Consider the subgraph $H_{(A,B)}^\vee$ of the dual graph H^\vee induced by $F \setminus h_{(A,B)}^{-1}(0)$. We say that $f \in F$ is *contained in sector* i if the vertices of H incident to f are all in sector i , and we say that a subgraph of $H_{(A,B)}^\vee$ is *almost contained*

⁵When we refer to “sectors” in this section, we mean the sectors defined in the right hand side of Figure 1.

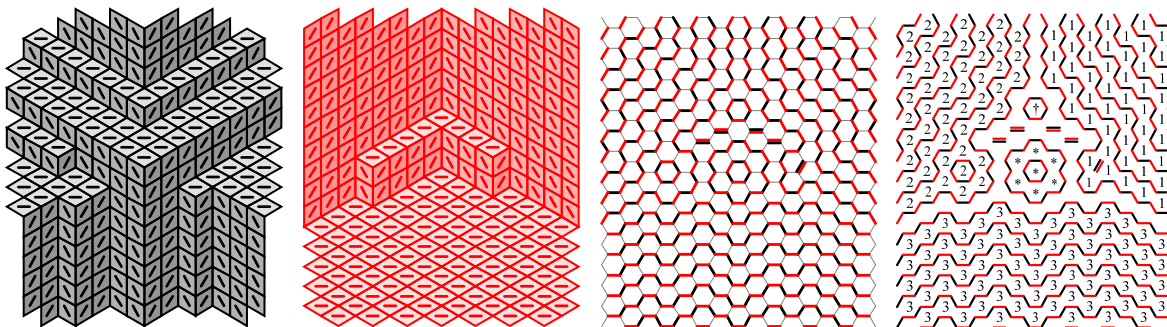


Figure 6: First: The dimer configuration M_A . Second: The dimer configuration M_B . Third: The superposition of M_A and M_B , a double-dimer configuration on H . Fourth: The labelled double-dimer configuration.

in sector i if it contains only finitely many faces that are not contained in sector i .

Algorithm 4.5. 1. If there is a connected component C of $H_{(A,B)}^\vee$ so that, given any i , C is not almost contained in sector i , terminate with failure.
 2. For each infinite connected component of $H_{(A,B)}^\vee$, there must be exactly one sector i almost containing it. Label the faces it contains by i .
 3. Label each finite connected component of $H_{(A,B)}^\vee$ by a freely chosen element of \mathbb{P}^1 .

For example, if we label the double-dimer configuration from Figure 6, we obtain the labelled double-dimer configuration shown in Figure 6. Observe that the paths in the double-dimer configuration in Figure 6 are “rainbow-like.” In other words, the paths are nested and start and end in the same sector.

Theorem 4.6. *Let (A, B) be an AB configuration. Then (A, B) is a labelled AB configuration if and only if $D_{(A,B)}$ has the property that each path starts and ends in the same sector.*

We prove Theorem 4.6 by proving that Algorithm 4.5 succeeds if and only if Algorithm 4.2 succeeds.

In order to apply the double-dimer analogue of Kuo’s graphical condensation, we must truncate our double-dimer configuration on the infinite honeycomb graph to obtain a *double-dimer configuration with nodes* on the $N \times N \times N$ honeycomb graph $H(N)$.

Definition 4.7. Let $G = (V_1, V_2, E)$ be a finite edge-weighted bipartite planar graph embedded in the plane with $|V_1| = |V_2|$. Let \mathbf{N} denote a set of special vertices called *nodes* on the outer face of G . A *double-dimer configuration* on (G, \mathbf{N}) is a multiset of the edges of G with the property that each internal vertex is the endpoint of exactly two edges, and each vertex in \mathbf{N} is the endpoint of exactly one edge.

Each double-dimer configuration is associated with a planar pairing of the nodes. On a finite graph, the notion that the paths are “rainbow-like” means that the pairing is *tripartite*.

Definition 4.8. A planar pairing σ is *tripartite* if the nodes can be divided into three circularly contiguous sets R, G , and B so that no node is paired with a node in the same set. We often color the nodes in the sets red, green, and blue, in which case σ is the unique planar pairing in which like colors are not paired.

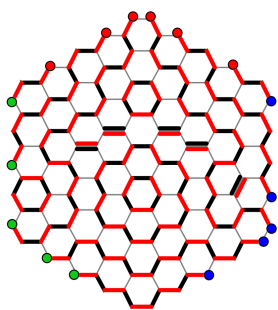


Figure 7

The process of truncating the infinite double-dimer configuration is straightforward and details are omitted here. Continuing our example, truncating the double-dimer configuration from Figure 6 to a double-dimer configuration on $H(5)$ produces the tripartite double-dimer configuration shown in Figure 7.

The set of nodes \mathbf{N} and the coloring of these nodes is determined by the partitions μ_1, μ_2 , and μ_3 , and this can be made explicit by using the Maya diagram associated to each partition.

We refer to the labelling and sectors of the graph $H(N)$ shown in Figure 1.

To determine the nodes in Sector i , we draw the Maya diagram associated to μ_i .

- In Sector 1, the blue nodes are the holes with positive coordinates and the red nodes are the beads with negative coordinates.
- In Sector 2, the red nodes are the holes with positive coordinates and the green nodes are the beads with negative coordinates.
- In Sector 3, the green nodes are the holes with positive coordinates and the blue nodes are the beads with negative coordinates.

4.3 The condensation identity for PT invariants

Let $Z_\sigma^{DD}(G, \mathbf{N})$ denote the weighted sum of all double-dimer configurations with a particular pairing σ . In [2], the first author showed that when σ is tripartite and certain other technical conditions hold we have the following:

$$\begin{aligned} & Z_\sigma^{DD}(G, \mathbf{N}) Z_{\sigma_5}^{DD}(G, \mathbf{N} - \{x, y, w, v\}) \\ &= Z_{\sigma_1}^{DD}(G, \mathbf{N} - \{x, y\}) Z_{\sigma_2}^{DD}(G, \mathbf{N} - \{w, v\}) + Z_{\sigma_3}^{DD}(G, \mathbf{N} - \{x, v\}) Z_{\sigma_4}^{DD}(G, \mathbf{N} - \{w, y\}) \end{aligned}$$

We apply this recurrence by *adding* nodes to the graph so that $\mathbf{N} = \tilde{\mathbf{N}} - \{a, b, c, d\}$ for four nodes a, b, c and d . We choose the four nodes as follows: Let a and b be the nodes in sector 1 labelled by $\max S_1^-$ and $\min S_1^+$, respectively. Similarly, we let c and d be the

nodes in sector 2 labelled by $\max S_2^-$ and $\min S_2^+$. Note that these nodes have the same coordinates as the vertices specified in Section 3.3 but the coordinate system is different (see Figure 1). Many details here have been omitted, due to space constraints.

Acknowledgements

We would like to thank Jim Bryan, Rick Kenyon, Rahul Pandharipande, Richard Thomas, Jim Propp, Karel Faber, Kurt Johansson, and frankly countless other geometers, probabilists and combinatorialists for helpful conversations.

References

- [1] A. Gholampour, M. Kool, and B. Young. “Rank 2 sheaves on toric 3-folds: classical and virtual counts”. *Int. Math. Res. Not. IMRN* 10 (2018), pp. 2981–3069.
- [2] H. Jenne. “Combinatorics of the Double-Dimer Model”. PhD thesis. University of Oregon, 2020.
- [3] H. Jenne, G. Webb, and B. Young. “The Combinatorial PT-DT Correspondence”. In preparation.
- [4] E. H. Kuo. “Applications of graphical condensation for enumerating matchings and tilings”. *Theoretical Computer Science* 319.1-3 (2004), pp. 29–57.
- [5] P. A. MacMahon. *Combinatory analysis*. Cambridge University Press, Cambridge, UK, 1915–16.
- [6] D. Maulik, N. Nekrasov, A. Okounkov, and R. Pandharipande. “Gromov–Witten theory and Donaldson–Thomas theory, I”. *Compositio Mathematica* 142.5 (2006), pp. 1263–1285.
- [7] D. Maulik, N. Nekrasov, A. Okounkov, and R. Pandharipande. “Gromov–Witten theory and Donaldson–Thomas theory, II”. *Compositio Mathematica* 142.5 (2006), pp. 1286–1304.
- [8] D. Maulik, A. Oblomkov, A. Okounkov, and R. Pandharipande. “Gromov–Witten/Donaldson–Thomas correspondence for toric 3-folds”. *Inventiones mathematicae* 186.2 (2011), pp. 435–479.
- [9] D. Maulik, R. Pandharipande, and R. P. Thomas. “Curves on K3 surfaces and modular forms”. *Journal of Topology* 3.4 (2010), pp. 937–996.
- [10] A. Okounkov, N. Reshetikhin, and C. Vafa. “Quantum Calabi–Yau and classical crystals”. *The unity of mathematics*. Vol. 244. Progr. Math. Birkhäuser Boston, Boston, MA, 2006, pp. 597–618.
- [11] R. Pandharipande and R. P. Thomas. “The 3-fold vertex via stable pairs”. *Geometry & Topology* 13.4 (2009), pp. 1835–1876.